

1 Simultaneous Measurement of Urban and Rural Particles in Beijing, Part II: Case Studies  
2 of Haze Events and Regional Transport

3 Yang Chen,<sup>1</sup> Guangming Shi,<sup>1,3</sup> Jing Cai,<sup>2</sup> Zongbo Shi,<sup>4,5</sup> Zhichao Wang,<sup>1</sup> Xiaojiang Yao,<sup>1</sup>  
4 Mi Tian,<sup>1</sup> Chao Peng,<sup>1</sup> Yiqun Han,<sup>2</sup> Tong Zhu,<sup>2</sup> Yue Liu,<sup>2</sup> Xi Yang,<sup>2</sup> Mei Zheng,<sup>2\*</sup> Fumo  
5 Yang,<sup>1,3\*</sup> and Kebin He<sup>6</sup>

6 <sup>1</sup>Chongqing Institute of Green and Intelligent Technology, Chinese Academy of Sciences,  
7 Chongqing 400714, China

8 <sup>2</sup>SKL-ESPC and BIC-ESAT, College of Environmental Sciences and Engineering, Peking  
9 University, Beijing 100871, China

10 <sup>3</sup> Department of Environmental Science and Engineering, College of Architecture and  
11 Environment, Sichuan University, Chengdu 610065, China

12 <sup>4</sup> School of Geography, Earth and Environmental Sciences, the University of Birmingham,  
13 Birmingham B15 2TT, UK

14 <sup>5</sup> Institute of Surface-Earth System Science, Tianjin University, Tianjin 300072, China

15 <sup>6</sup> School of Environment, Tsinghua University, Beijing 100084, China

16 Corresponding to Fumo Yang (fmyang@scu.edu.cn) and Mei Zheng  
17 (mzheng@pku.edu.cn)

18 Abstract

19 Two parallel field studies were conducted simultaneously at both urban and rural sites in  
20 Beijing from 11/01/2016 to 11/29/2016. Online single-particle chemical composition  
21 analysis was used as a tracer system to investigate the impact of heating activities and  
22 formation of haze events. Central heating elevated EC-Nit, EC-Nit-Sul, and ECOC-Nit  
23 levels by 1.5–2.0 times due to the increased use of coal in the urban areas. However, in the  
24 rural areas, residential heating which mainly consumes low-quality coal and biomass  
25 burning elevated ECOC-Nit-Sul, Nak-Nit, and OC-Sul levels by 1.2–1.5 times. Four severe  
26 haze events (hourly  $PM_{2.5} > 200 \mu g m^{-3}$ ) occurred at both sites during the studies. In each  
27 event, a pattern of “transport and accumulation” was found. In the first stage of the pattern,  
28 particles were regionally transported from the south or southwest and accumulated under  
29 air stagnations, creating significant secondary formation, then  $PM_{2.5}$  boosted up to  $300 \mu g$   
30  $m^{-3}$ . At both sites, the severe haze occurred due to different patterns of local emission,  
31 transport, and secondary processes. At PG, the sulfate-rich residential coal burning  
32 particles were dominant. The regional transport between PG and PKU was simulated using  
33 the WRF-HYSPLIT model, confirming that the transport from PG to PKU was significant,  
34 but PKU to PG occurred occasionally. These cases can explain the serious air pollution in  
35 the urban areas of Beijing and the interaction between urban and rural areas. This study  
36 can provide references for enhancing our understanding of haze formation in Beijing.

37 Keywords: urban; regional; single particle; transport; pollution event

38

## 39 **1. Introduction**

40 The Beijing-Tianjin-Hebei (BTH) area in China has been suffering from extreme haze  
41 events caused by high concentrations of  $\text{PM}_{2.5}$  ( $> 200 \mu\text{g m}^{-3}$ ) since 2013 (Guo et al., 2014).  
42 Studies have been performed to understand the formation of such massive haze events in  
43 Beijing (Tian et al., 2014; Quan et al., 2013; Che et al., 2014; He et al., 2015). Traffic,  
44 cooking, and coal combustion emissions accounted for 41–59% of the total submicron  
45 organic aerosols, and the remainder was secondary organic aerosols (Sun et al., 2014).  
46 Model studies suggest that temperature inversion, low boundary layer, and transported  
47 pollutants cause the local accumulation of  $\text{PM}_{2.5}$  in urban areas (Zhang et al., 2015). In  
48 short, significant local emissions, unfavorable meteorological conditions, and regional  
49 transport play essential roles in accumulating  $\text{PM}_{2.5}$ .

50 There are unresolved issues surrounding whether the rapid boosting of PM in Beijing is  
51 due to local secondary aerosol formation or transport. Wang et al. (2016) have proposed  
52 that the accumulation of nitrates is dominant at the beginning of haze events, and then  
53 sulfate increases because  $\text{SO}_2$  is oxidized into sulfate in ammonium-rich conditions.  
54 Moreover, Cheng et al. (2016) have suggested that  $\text{NO}_2$  could oxidize  $\text{SO}_2$  to sulfate on the  
55 surface of alkali aerosols. However, Li et al. (2015) have argued that regionally transported  
56  $\text{PM}_{2.5}$  is a significant cause of severe haze. Last but not least, Sun et al (2013) and (2014)  
57 have proposed that both local formation and regional transport are causing factors. Except  
58 for model studies, most field studies have focused on urban areas in Beijing, with limited  
59 attention to rural areas. The characterization of rural PM is also essential to understanding  
60 the evolution of particulate haze events.

61 The cold winter results in the necessity of heating, consequently impacting the air quality  
62 in BTH (Sun et al., 2014). In urban areas, central heating systems use coal or natural gas,  
63 while rural households use coal or biofuel for heating and cooking. Residential emissions  
64 in Beijing reach about 4 million tons, mainly caused by low-efficiency coal combustion  
65 (Li et al., 2015). Coal combustion organic aerosols (CCOA) account for 20–32% of total  
66 submicron OA in Beijing (Sun et al., 2014; Sun et al., 2013a). However, whether CCOA  
67 is contributed by central or household heating remains unclear. Notably, central and  
68 household heating release distinct particles due to different burning conditions (Lee et al.,  
69 2005; Chagger et al., 1999). Therefore, analyzing household heating and cooking emissions  
70 in rural areas is also beneficial for understanding the source of urban PM<sub>2.5</sub> in Beijing.

71 SPAMS has proven a useful tool for characterizing the single-particle chemical  
72 composition, mixing state, and processing of atmospheric particles (Chen et al., 2019a).  
73 Single-particle chemical composition and mixing state can be used as a tracing system to  
74 explore the sources and origins of unique particle types (Chen et al., 2019b; Li et al., 2016).  
75 For example, by combining meteorological parameters, we can determine the sources and  
76 transport conditions of specific particle types (Chen et al., 2018; Chen et al., 2020).

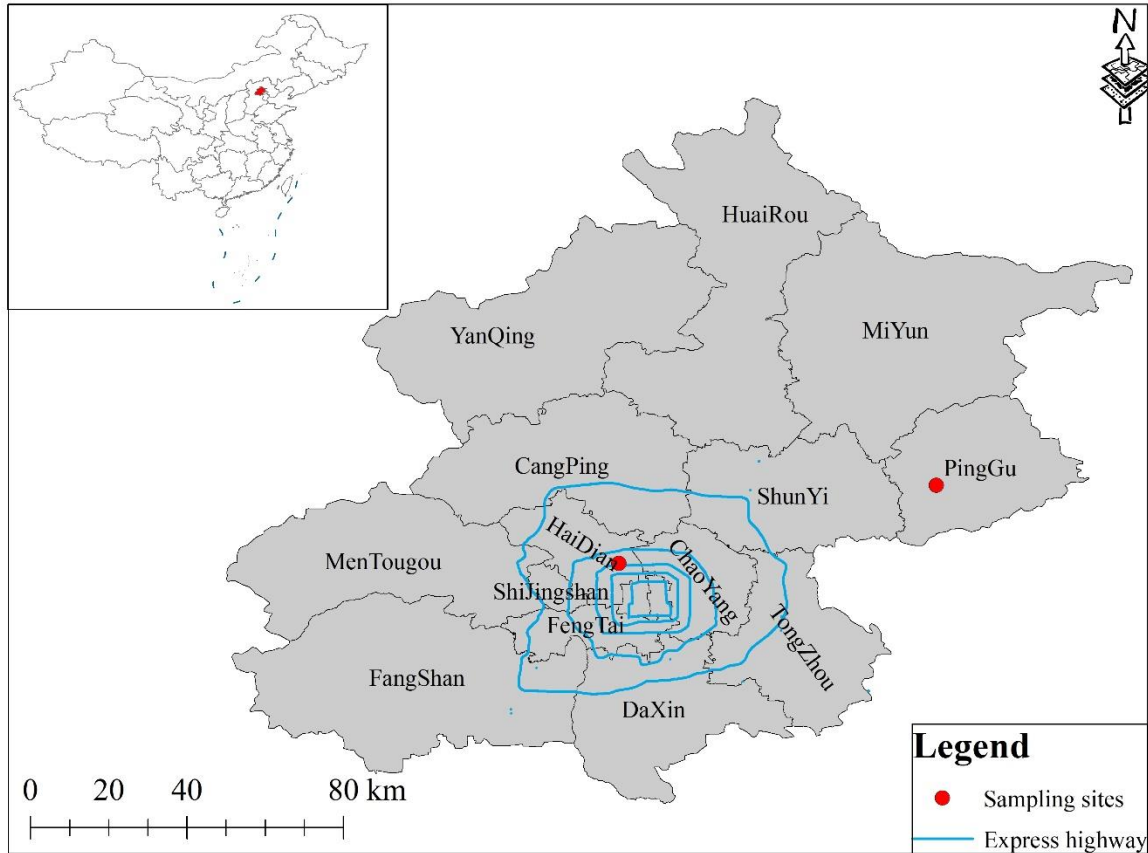
77 As mentioned in Part I (Chen et al., 2020), two SPAMSs were deployed simultaneously at  
78 Peking University (PKU) and Pinggu (PG) to monitor urban and rural particles in the  
79 Beijing region. In Part II, the resolved particle types are used to trace the evolution,  
80 transport, and formation of pollution events. The detailed analysis of haze events and  
81 effects of heating activities are addressed. Combining field measurements and model

82 studies, the interactions between the two sampling sites, representing urban and rural  
83 eastern areas, are systematically analyzed.

## 84 **2. Methodology**

### 85 **2.1 Sampling sites, instrumentation, and data analysis**

86 Please refer to Part I and Support Information for the detail (Chen et al., 2020). Briefly, the  
87 field studies were performed simultaneously at Peking University (PKU) (116.32°E,  
88 39.99°N) and Pinggu (PG) (117.05°E, 40.17°N) from 11/01/2016 to 11/29/2016 (Figure  
89 1). The detail description of these two sites are available at (Chen et al., 2020). The two  
90 sites represent both typical urban and rural areas, respectively. The local meteorological  
91 data is retrieved from the local meteorological offices. Two SPAMSs (0515, Hexin Inc.,  
92 Guangzhou, China) were deployed at both sites for parallel measurements. SPAMS  
93 generates single particle mass spectra from the captured individual particles. The technical  
94 description of SPAMS is available in the literature (Li et al., 2011). A neural network  
95 algorithm based on adaptive resonance theory (ART-2a) was applied for clustering particle  
96 types in the datasets (Song et al., 1999). During the clustering procedure, the relative peak  
97 areas (RPA) of sulfate and nitrate are considered. A criterion of RPA >0.1 is used to  
98 identify the nitrate-rich (-Nit), sulfate-rich (-Sul), or both. Based on the strategy, 20 and 19  
99 particle types were identified at PKU and PG respectively.



100

101

Figure 1 Map of the sampling sites.

102

## 2.2 Dispersion model

103

A WRF-HYSPLIT (Weather Research and Forecasting - Hybrid Single Particle

104

Lagrangian Integrated Trajectory) coupling model was used to describe the air parcel

105

movement between PKU and PG. The description of the model is available at

106

<https://www.arl.noaa.gov/hysplit/inline-wrf-hysplit-coupling/>. The HYSPLIT dispersion

107

simulations were driven by the meteorological data fields from the WRF model version

108

3.8. The WRF domains are shown in Figure 2. The innermost domain was configured to

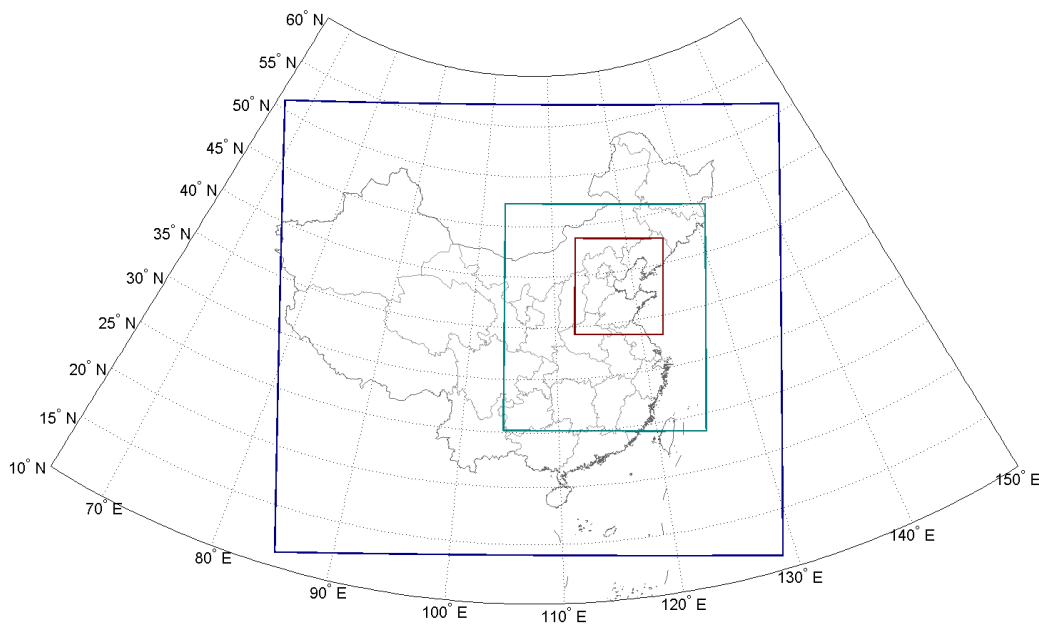
109

cover northern China with a horizontal resolution of 3 km and 35 vertical layers. The

110

longwave and shortwave radiation schemes were set as the RRTMG and Dudhia scheme

111 respectively. The Yonsei University (YSU) scheme was used for the PBL parameterization.  
112 For the microphysics, the Morrison 2-moment scheme was adopted. NCEP FNL (National  
113 Centers for Environmental Prediction, final) data with a resolution of  $1^\circ \times 1^\circ$  was employed  
114 as initial and boundary conditions. The WRF simulation was initialized as a “cold start” at  
115 0000 UTC each day and ran for 36 hours. The first 12 hours were discarded as model spin-  
116 up time, and the output for the following 24 hours was retained. This process was repeated  
117 to produce continuous meteorological data fields for the whole experimental period. The  
118 HYSPLIT was set to release 10,000 Lagrangian particles within one hour at PKU and PG,  
119 10 m above ground level. The concentration of released particles was simulated with one  
120 vertical layer extending from 0 to 1,000 m above ground level.



121

122 Figure 2. Spatial configuration of domains used for WRF simulation.

## 123 **3. Results and Discussion**

### 124 **3.1 Particle type description**

125 We observed five particle categories at both sites: elemental carbon (EC), organic carbon  
126 (OC), internal-mixed EC and OC (ECOC), potassium-rich (K-rich), and metals. According  
127 to their different stages of atmospheric processing, the five categories can be divided into  
128 up to 20 particle types, as shown in Table 1. Particles with relative peak areas of sulfate  
129 and nitrate greater than 0.1 were marked with nitrate (-Nit) or sulfate (-Sul), respectively,  
130 or both (-Nit-Sul). The typical single-particle mass spectra of all particle types are available  
131 in Supportive Information and. Besides, the suffixes “\_PKU” and “\_PG” are used when  
132 the same particles appear. The higher relative abundance of secondary species indicates the  
133 particles are more aged (Chen et al., 2020).

134 As described in Part I, we performed a responding analysis of meteorological factors (e.g.  
135 wind speed and wind direction) and hourly number counts of observed particles at both  
136 sites. At PKU, the following particle types were local: EC-Nit, EC-Nit-Sul, ECOC-Nit-  
137 Sul, Ca-rich, and ECOC-Nit. These particles arrived at PKU with no unique orientations,  
138 at low wind speed (commonly  $< 2 \text{ m s}^{-1}$ ) and with clear diurnal patterns. On the contrary,  
139 parts of OC-Nit, OC-Sul, NaK-Nit, and NaK-Nit-Sul responded to unique wind directions,  
140 implying that these particle types were regionally transported. At PG, all particle types  
141 showed patterns that were both local and regional. For example, OC, ECOC, OC-Nit-Sul,  
142 and ECOC-Nit-Sul came from the local area, northeast, and southwest. Universal patterns  
143 can be used to determine the mechanisms of pollution event formation when combined  
144 with unique cases.



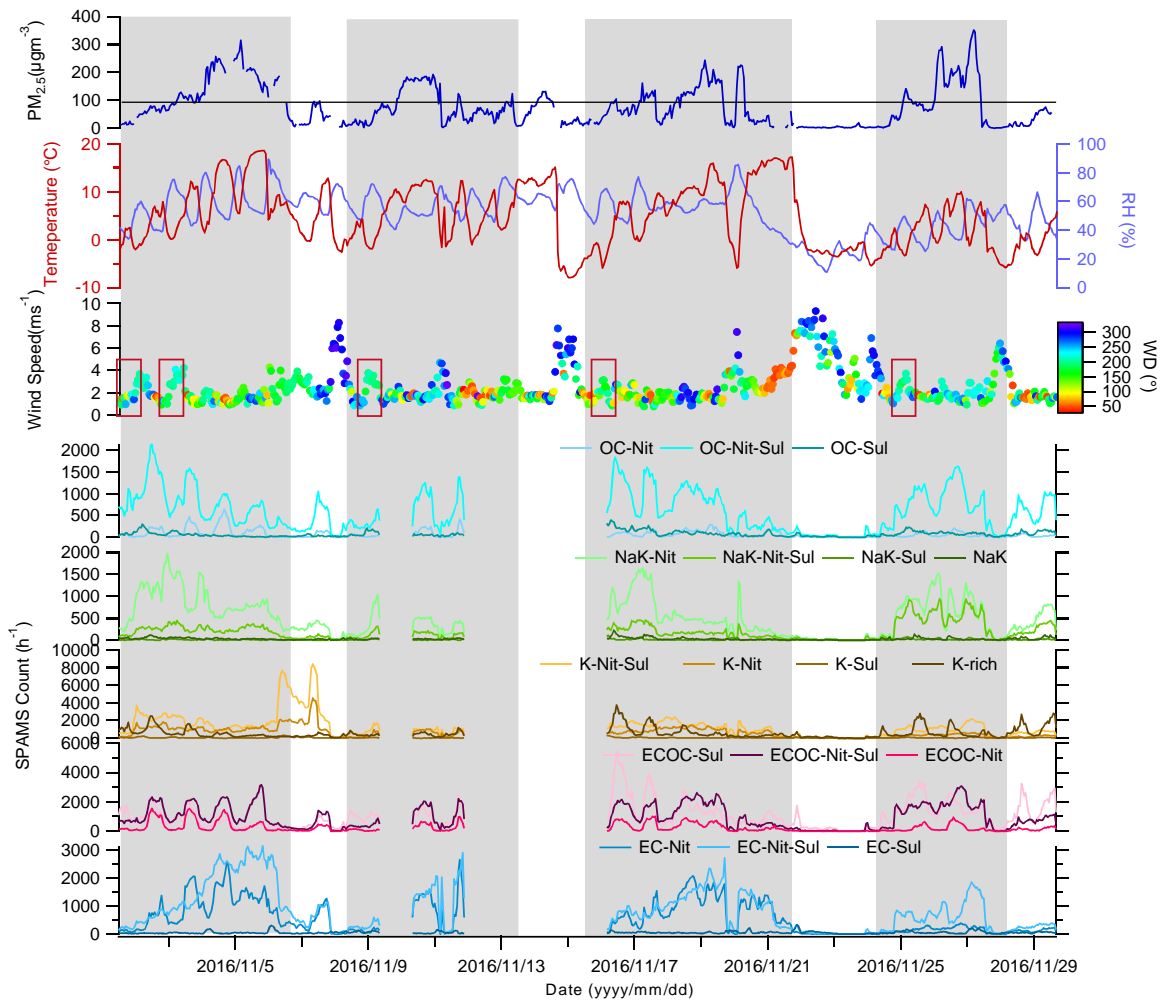
145 Table 1. Particle types and their relative fractions and chemical composition

	Both	PKU	PG	Chemical Composition*	
EC	EC-Nit	7.0	2.0	$C_n^+$ , $C_n^-$ , $HSO_4^-$ , $NO_2^-$ , $NO_3^-$	
	EC-Nit-Sul	10.5	3.5		
	EC-Sul	0.7	0.1		
ECOC	ECOC-Nit-Sul	12.0	18.6	$C_n^+$ , $C_n^-$ , $C_xH_y^+$ , $C_xH_yO_z^+$ $HSO_4^-$ , $NO_3^-$	
	ECOC-Sul	12.7	9.8		
K-rich	K-rich	7.2	6.4	$K^+$ , $NH_4^+$ , $HSO_4^-$ , $NO_3^-$ $NO_2^-$	
	K-Nit	8.0	8.2		
	K-Nit-Sul	16.0	1.9		
	K-Sul	0.6	4.5		
NaK	NaK	0.4	1.8	$Na^+$ , $K^+$ , $NH_4^+$ , $HSO_4^-$ , $NO_3^-$	
	NaK-Nit	6.4	1.7		
	NaK-Nit-Sul	2.5	1.9		
	NaK-Sul	0.2	0.4		
OC	OC-Nit-Sul	7.4	21.3	$C_xH_y^+$ , $C_xH_yO_z^+$ , $NH_4^+$ $HSO_4^-$ , $NO_3^-$ $Cl^-$	
	OC-Sul	0.9	6.9		
	Ca-dust	0.4	0.1		
Fe	Fe-rich	3.1	1.8	$Fe^+$ , Org, $HSO_4^-$ , $NO_3^-$ TMA, $NH_4^+$ , $HSO_4^-$ , $NO_3^-$	
	ECOC-Nit	3.1%			
	OC-Nit	0.9%			
	K-Amine-Nit-Sul	0.1%			
	ECOC		5.9%		$C_n^+$ , $C_n^-$ , $C_xH_y^+$ , $C_xH_yO_z$
	OC		3.3%		$C_xH_y^+$ , $C_xH_yO_z$

146 \* chemical species with ionic relative peak area >0.1

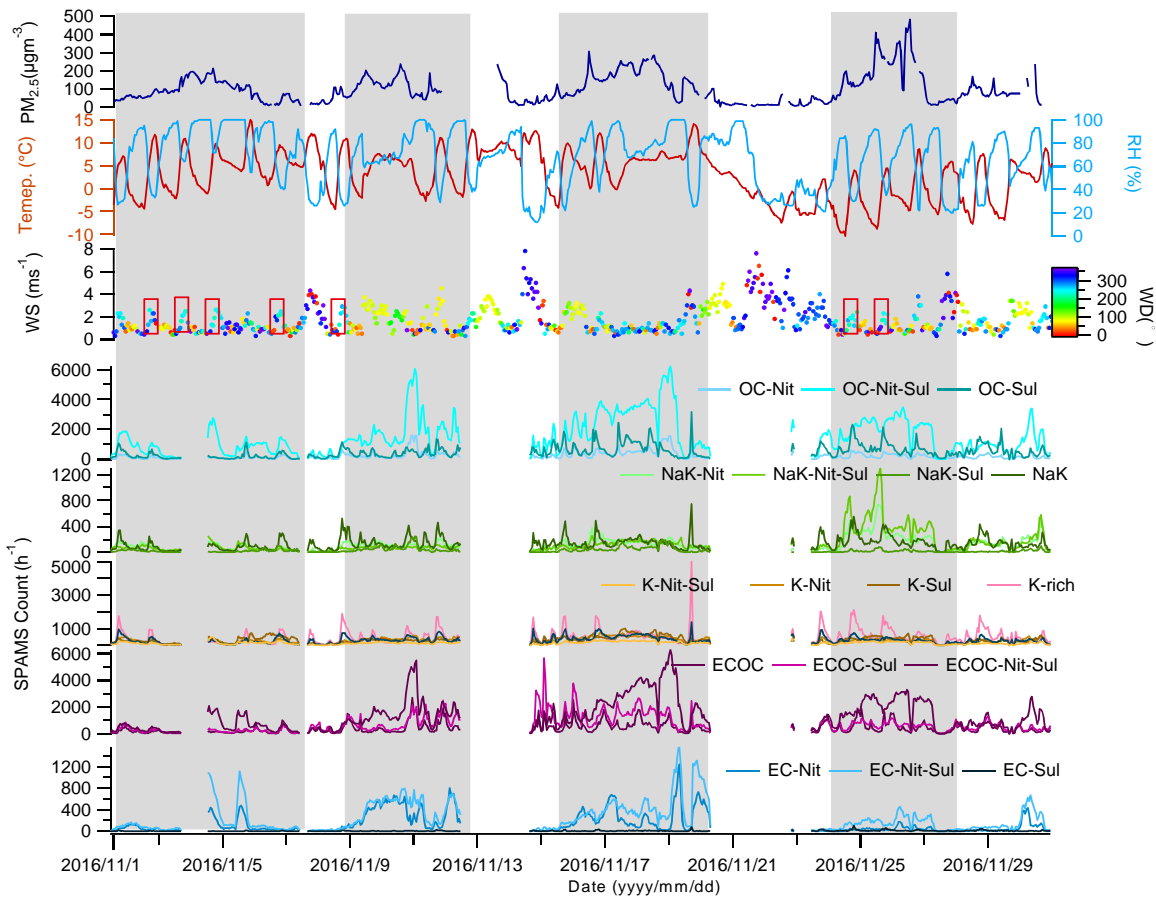
### 147 3.2 Overview of haze events

148 Figures 3 and 4 show the overview of PM<sub>2.5</sub>, meteorology parameters, and time trends of  
 149 particles at PKU and PG respectively. There were four parallel haze events during the  
 150 observation period: 11/01/2016–11/07/2016 (E1), 11/09/2016–11/15/2016 (E2),  
 151 11/15/2016–11/22/2016 (E3), and 11/25/2016–11/28/2016 (E4).



152

153 Figure. 3. Time trends of PM<sub>2.5</sub>, temperature, relative humidity, wind direction, wind speed,  
 154 and single particle types at PKU. The rectangles indicate the transport of regional particles.



155

156 Figure 4. Time trends of PM<sub>2.5</sub>, temperature, relative humidity, wind direction, wind speed,  
 157 and single particle types at PG. The rectangles indicate the transport of regional particles.

158 The pattern of single-particle chemical composition, represented by normalized number  
 159 fractions of particle types in different periods, is used to describe PM characteristics. The  
 160 correlations of normalized number fractions during events at PKU and PG are shown in  
 161 Tables 2 and S3. E1\_PKU was well correlated with Clear1 ( $R = 0.90$ ) and E2\_PKU ( $R =$   
 162  $0.86$ ), but poorly correlated with Clear2 ( $R = 0.38$ ) and E4 ( $R = 0.64$ ). This is because  
 163 E1\_PKU and E2\_PKU occurred before the heating period, but E4\_PKU occurred after  
 164 (11/15/2016). The chemical compositions of the four events at PG are highly correlated

165 with each other (all  $R_s > 0.90$ , Table S3). These results indicate that the chemical  
166 composition patterns changed significantly at PKU, but insignificantly at PG.

167 Table 2. Correlations of number fractions of particle types in different events at PKU.

	E1	Clear1	E2	Clear2*	E4
E1	1				
Clear1	0.90	1			
E2	0.86	0.91	1		
Clear2	0.38	0.70	0.58	1	
E4	0.64	0.81	0.83	0.76	1

168 Note: The chemical composition of E3 is unavailable.

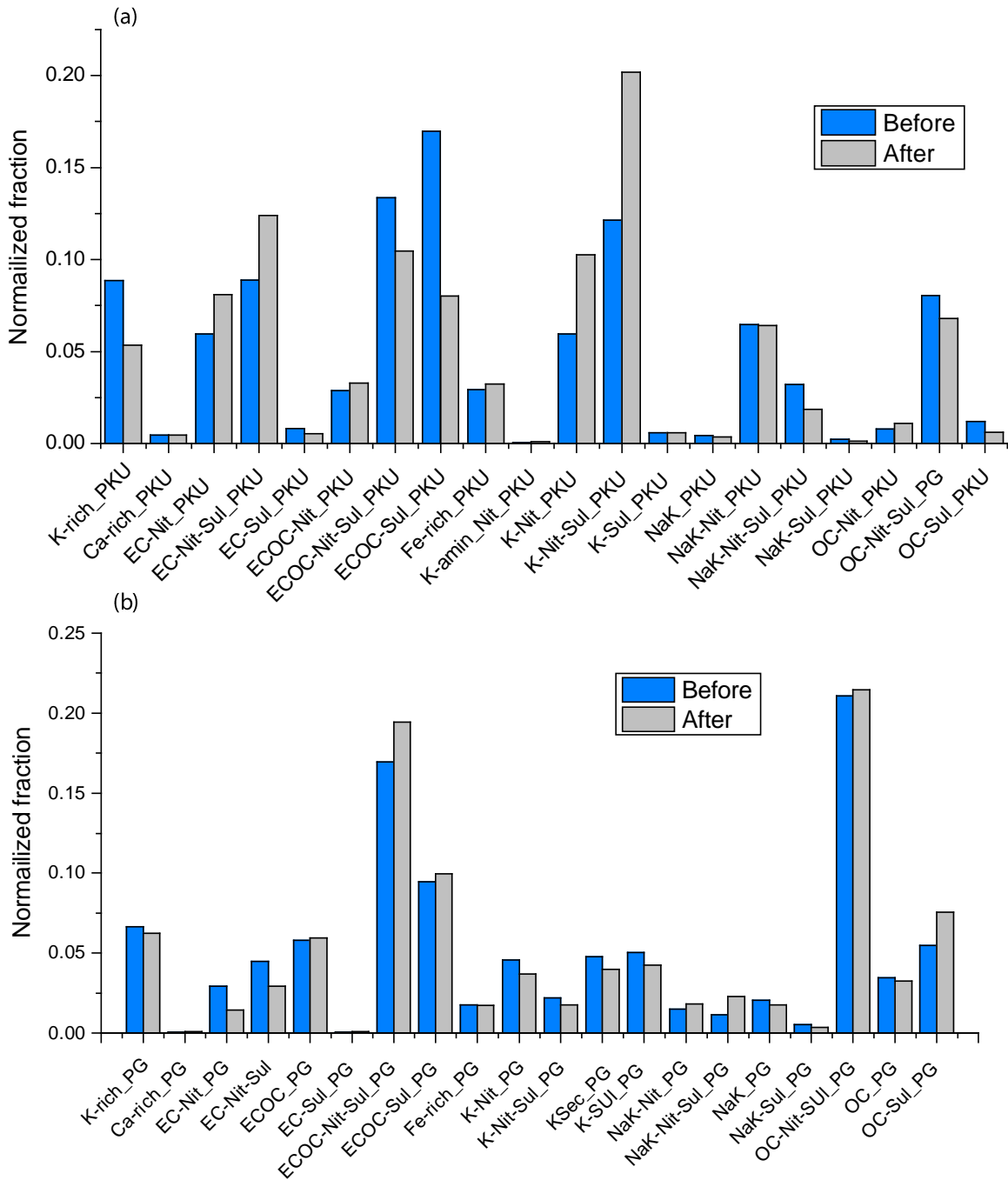
169 **3.3 Influence of heating activities**

170 Central heating began on 11/15/2016 in the urban area, while residential heating in the rural  
171 area had no distinct starting day. As such, the shift in emissions due to the increased use of  
172 solid fuel directly affected the particulate chemical composition. As shown in Figure 5, the  
173 normalized fractions of EC-Nit\_PKU, EC-Nit-Sul\_PKU, and OC-Nit\_PKU increased by  
174 about 1.5 times. EC-Nit\_PKU and EC-Nit-Sul\_PKU came from multiple local sources, one  
175 of which was coal burning in boilers (Xu et al., 2018). In addition, high EC concentrations  
176 have been observed during the heating period each year for decades (Chen et al., 2016b).  
177 The mass spectra of OC-Nit particles were composed of a series of ion fragments of  
178 polycyclic aromatic hydrocarbons (PAHs). The results are consistent with organic aerosols  
179 from coal burning in AMS-related studies (Wang et al., 2019; Sun et al., 2013b).  
180 Additionally, PM<sub>2.5</sub>-bound PAHs increased by three times when the heating period began  
181 in Beijing (Zhang et al., 2017). The results also suggest the potential health risks of coal  
182 burning in wintertime in Beijing (Linak et al., 2007; Chen et al., 2013).

183 Biomass burning (BB) has been proven as a significant source of PM<sub>2.5</sub> in Beijing (Sun et  
184 al., 2013b; Sun et al., 2014), accounting for 9–12% (Liu et al., 2019). Anthropogenic BB,  
185 e.g. burning household biofuel, is prohibited in urban areas, but common in the areas  
186 surrounding Beijing. Most BB-related particles such as K-rich, K-Nit, and K-Nit-Sul at  
187 PKU were regional (Part I)(Chen et al., 2020). Not surprisingly, K-Nit\_PKU and K-Nit-  
188 Sul\_PKU both increased to 1.7 times after 11/15/2016. Interestingly, K-Amine-Nit\_PKU  
189 increased by 2.3 times after the heating period began, suggesting that BB is also a source  
190 of particulate amines in Beijing (Chen et al., 2019b).

191 After 11/15/2016, NaK-Nit-Sul\_PG, Ca-rich\_PG, and OC-Sul\_PG increased by 1.96, 1.30,  
192 and 1.47 times respectively. As described above, in rural areas, low-quality coal is  
193 commonly used for residential heating and cooking, resulting in abundant EC-Sul, OC-Sul,  
194 and NaK-Nit-Sul (Xu et al., 2018; Chen et al., 2016a). Interestingly, Ca-rich particles that  
195 were well correlated with OC-Sul ( $R = 0.79$ ) also increased, possibly due to flying ash from  
196 coal stoves.

197 A number of studies have reported contributions of coal burning to the submicron PM in  
198 urban areas of Beijing. According to these mass-based studies, PM-bound PAHs, chloride,  
199 sulfate, nitrate, and lead were markers from emissions of coal burning (Xu et al., 2018; Sun  
200 et al., 2014; Ma et al., 2016; Zhang et al., 2019). Our result shows that these species were  
201 internally mixed as the ECOC particles. In particular, the household heating in PG released  
202 significant fractions of ECOC particles that arrived in the urban areas of Beijing. Likewise,  
203 K-rich particles from BB also transport to the urban areas of Beijing. Conclusively, [control](#)  
204 [of emissions from household heating](#) is also a key to improve the air quality in Beijing.



205

206 Figure 5. Variation of particle number fractions at PKU and PG before and after the heating

207 period 2017.

### 208 3.4 Case studies: Haze events at PKU

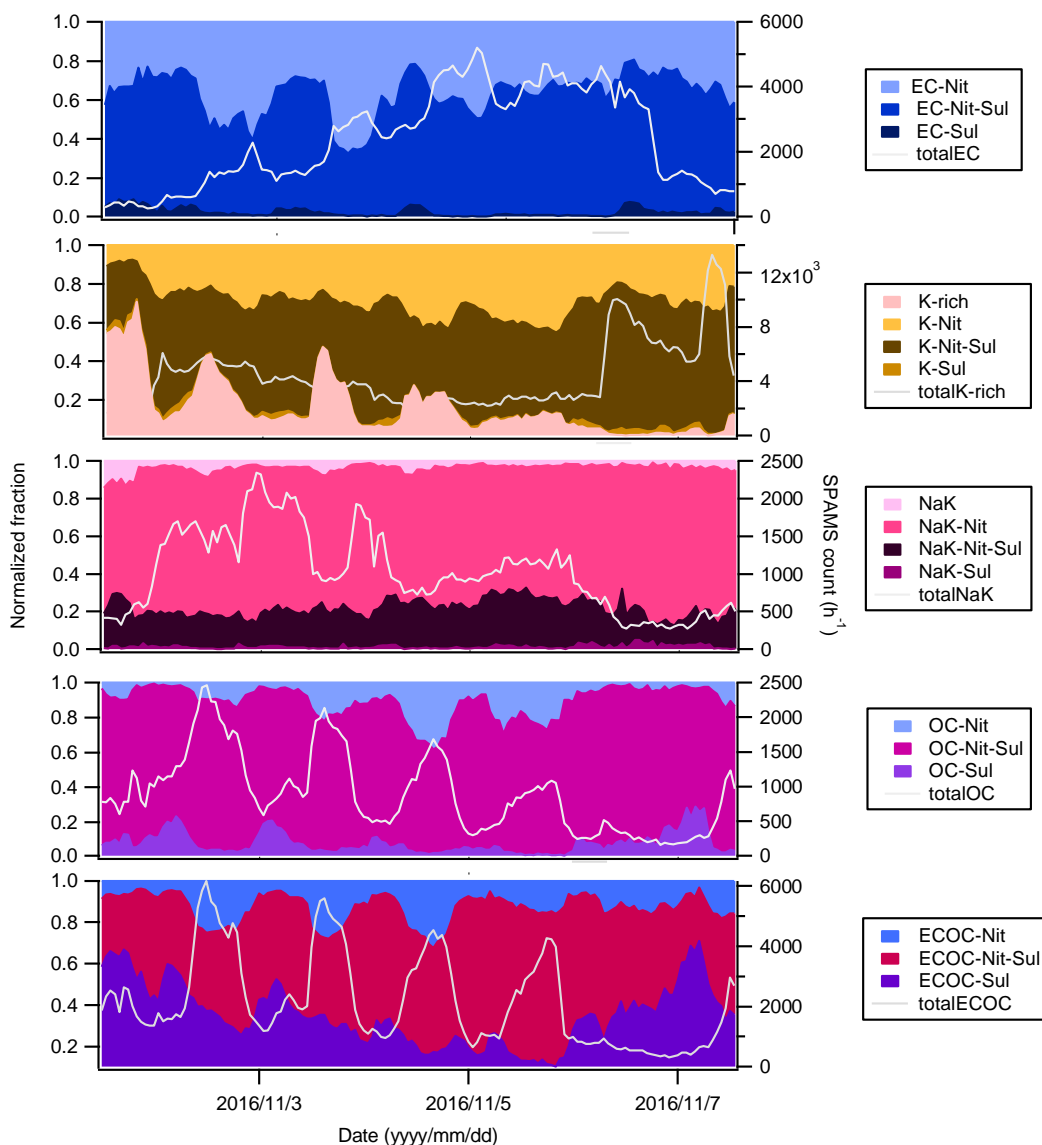
209 As shown in Figure 3, before  $PM_{2.5}$  increased to  $100 \mu g m^{-3}$  during E1\_PKU, two processes  
210 of  $PM_{2.5}$  transport were observed. The first process was from 12:00 on 11/01/2016 to 2:00  
211 on 11/02/2016, in which OC-Nit-Sul, K-Nit-Sul, K-Nit, NaK-Nit, K-Nit-Sul increased  
212 dramatically as the southern wind speed increased from  $1.3 m s^{-1}$  to  $3.7 m s^{-1}$ . The wind  
213 speed then decreased to  $1.2 m s^{-1}$  until 16:00 on 11/02/2016, and the accumulation of  $PM_{2.5}$   
214 resulted in a concentration of  $67 \mu g m^{-3}$ . The second process occurred from 17:00 on  
215 11/02/2016 to 16:00 on 11/03/2016. Severe accumulation then started at 1:00 on  
216 11/04/2016, with an elevating trend of RH, reaching the highest  $PM_{2.5}$  level of  $314 \mu g m^{-3}$   
217 at 03:00 on 11/05/2016. After that, the wind dispersed the  $PM_{2.5}$  to  $11 \mu g m^{-3}$  at 17:00 on  
218 11/06/2016. In short, regional particles were transported from the south or southwest, then  
219 the accumulation of  $PM_{2.5}$  began. The accumulation of pollutants was accompanied by  
220 secondary aerosol formation, causing severe haze events.

221 During the events at PKU (Figure 3), particles transported from the south and southwest  
222 were observed and labeled with red rectangles. During E4\_PKU, the  $PM_{2.5}$  concentration  
223 increased from  $6 \mu g m^{-3}$  to  $122 \mu g m^{-3}$  between 15:00 on 11/24/2016 and 3:00 on  
224 11/25/2016 due to the southern wind, which brought abundant NaK-Nit, NaK-Nit-Sul,  
225 ECOC-Nit-Sul, and EC-Nit-Sul. Notably, regional particles were dramatically different  
226 from those of E1\_PKU due to the heating period. Then, under stagnant air conditions, the  
227 accumulation began at 22:00 on 11/25/2016 and lasted until 03:00 on 11/26/2016, with  
228  $PM_{2.5}$  levels reaching  $281 \mu g m^{-3}$ . At this stage, such local particles as OC-Nit-Sul, ECOC-  
229 Nit-Sul, and ECOC-Nit also showed accumulation and local emissions, while both the K-  
230 rich and NaK families showed a pattern of transport and accumulation (Figures 6 and 7).

231 As shown in Figure 6, which gives an integrated view of related particle types in urban  
232 Beijing, three types of particle evolution are distinguished during E1. First, EC particles,  
233 including EC-Nit, EC-Nit-Sul, and EC-Sul, show trends of accumulation, but with clear  
234 patterns of emissions, suggesting a pattern of emission and accumulation. Second, for  
235 regional particles such as the K-rich and NaK families, the processes of transport and  
236 accumulation were identified, with significant accumulation but unclear diurnal patterns.  
237 Third, the OC and ECOC families illustrated clear diurnal patterns of local emission and  
238 evolution. Notably, during the development of E1, the fractions of aged ECOC-Nit-Sul  
239 increased from 20% to 83%, suggesting that significant secondary processing occurred.

240 Due to the nature of SPAMS, the quantitative measurement of secondary formation is  
241 unavailable. Fortunately, as an integrated and extensive project, APHH-Beijing also  
242 included the online monitoring of the chemical composition of PM<sub>2.5</sub>. For example, during  
243 the transport stage of E4\_PKU, PM<sub>2.5</sub> was composed of 60% organic matter (OM) and 40%  
244 total nitrate, sulfate, and ammonium. During the accumulation stage, sulfate, nitrate, and  
245 ammonium levels were boosted up to 123  $\mu\text{g m}^{-3}$  (63%) together (Liu et al., 2019). Wang  
246 et al. (2019) also reported that, during the accumulation stage of E4\_PKU, the elevation of  
247 secondary OOA1 and OOA2 was significant.





248

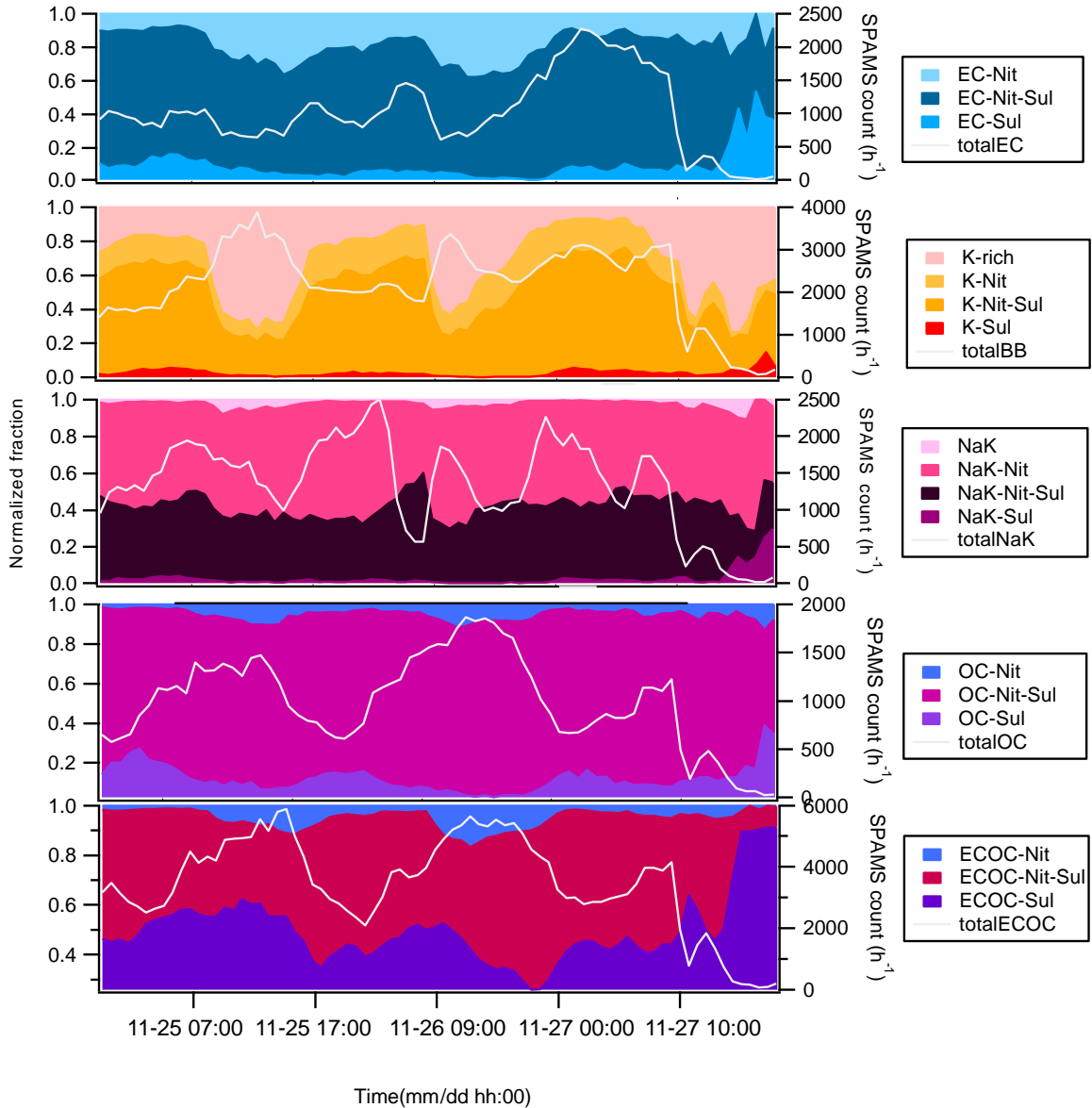
249 Figure 6. Time trends of number fractions of particle types (left) and hourly counts of  
 250 particle families (EC, BB, NaK, OC, and ECOC, right) during Pollution Event 1 (E1 11/01–  
 251 11/08) at PKU.

252 In the most recent study of aerosol-radiation feedback deterioration in Beijing during  
 253 wintertime, Wu et al. (2019) proposed that the increase of near-surface  $PM_{2.5}$  from 10 to  
 254  $200 \mu g m^{-3}$  can result in a decrease of the planetary boundary layer (PBL) from 1,500 m to  
 255 400 m, the decrease consequently contributes to  $PM_{2.5}$  concentration by 20%. However, a

256 20% difference cannot explain that PM<sub>2.5</sub> concentration increased from 100 μg m<sup>-3</sup> to 300  
257 μg m<sup>-3</sup>. Moreover, when PM<sub>2.5</sub> exceeded 200 μg m<sup>-3</sup>, the height of the PBL remained at  
258 400–500 m and air stagnation occurred with weak horizontal wind and inactive advection.  
259 Zhong et al. (2017) observed that weak temperature inversion occurred at the same period,  
260 and near-surface RH increased after southerly transport, along with decreased vertical wind  
261 speed and increased RH during winter. Air stagnation was also observed in this study with  
262 low wind speed and high RH (Figure 2). Based on the evidence of chemical evolution, the  
263 southerly transport of PM was strongly connected to pollution events at PKU.

### 264 **3.5 Case studies: Haze events at PG**

265 A pollution event occurred at PG (E1\_PG) from 11/01 to 11/08. During this period, a  
266 similar pattern of transport and accumulation as E1\_PKU was also observed. At the  
267 beginning of each pollution event, there was also a transport process of particles from the  
268 southwest (Figure 4); when the wind speed reached < 2 m s<sup>-1</sup>, accumulations began, and  
269 the haze dispersed with the elevating wind speed. The development of haze events was  
270 similar, and Figure 4 lists all the favorable wind directions for transport marked with red  
271 rectangles. As shown in Figure 9, EC-Nit and EC-Nit-Sul showed unclear diurnal patterns,  
272 indicating that both particle types were transported regionally. K-rich, NaK, OC, and  
273 ECOC had clear diurnal heating and cooking patterns, suggesting that local sources were  
274 dominant. Such aged particle types as OC-Nit-Sul and ECOC-Nit-Sul increased due to  
275 local aging processes during E1\_PG. Therefore, E1\_PG was mainly driven by the input of  
276 particles, local emissions, and accumulation. Moreover, the relative abundance of ECOC-  
277 Nit-Sul increased twofold from 2:00 on 11/03/2016 to 12:00 on 11/03/2016, suggesting the  
278 contribution of secondary formation (Figure 8).



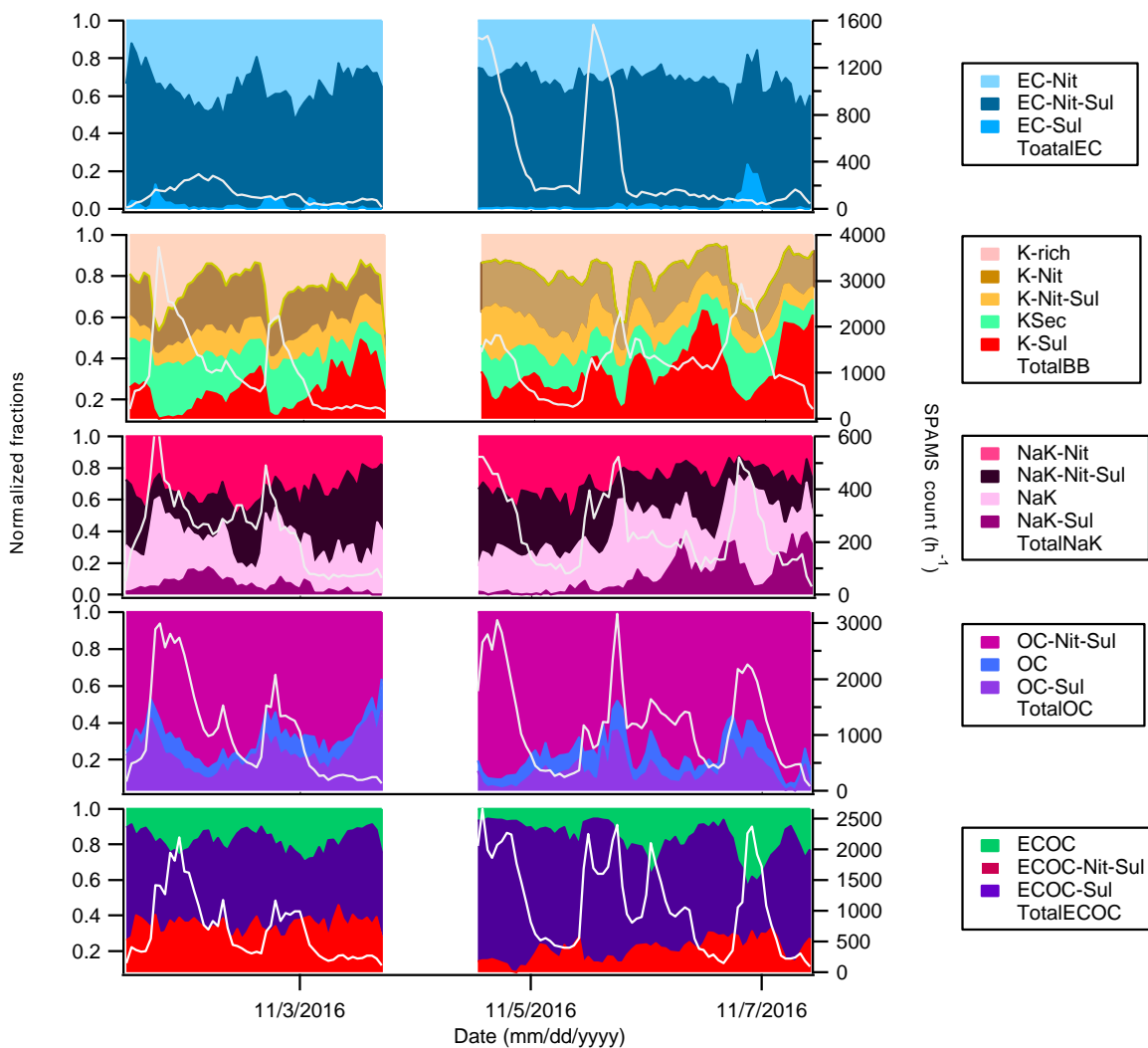
280

281 Figure 7. Normalized time trends of number fraction of particle types (left) and hourly  
 282 counts of particle families (EC, BB, NaK, OC, and ECOC, right) during Pollution Event 4  
 283 (E4) at PKU.

284 Both E1\_PG and E1\_PKU had patterns of transport and accumulation, but the transported  
 285 particles were different; for example, at the PG site, the appearance of EC-Nit and EC-Nit-

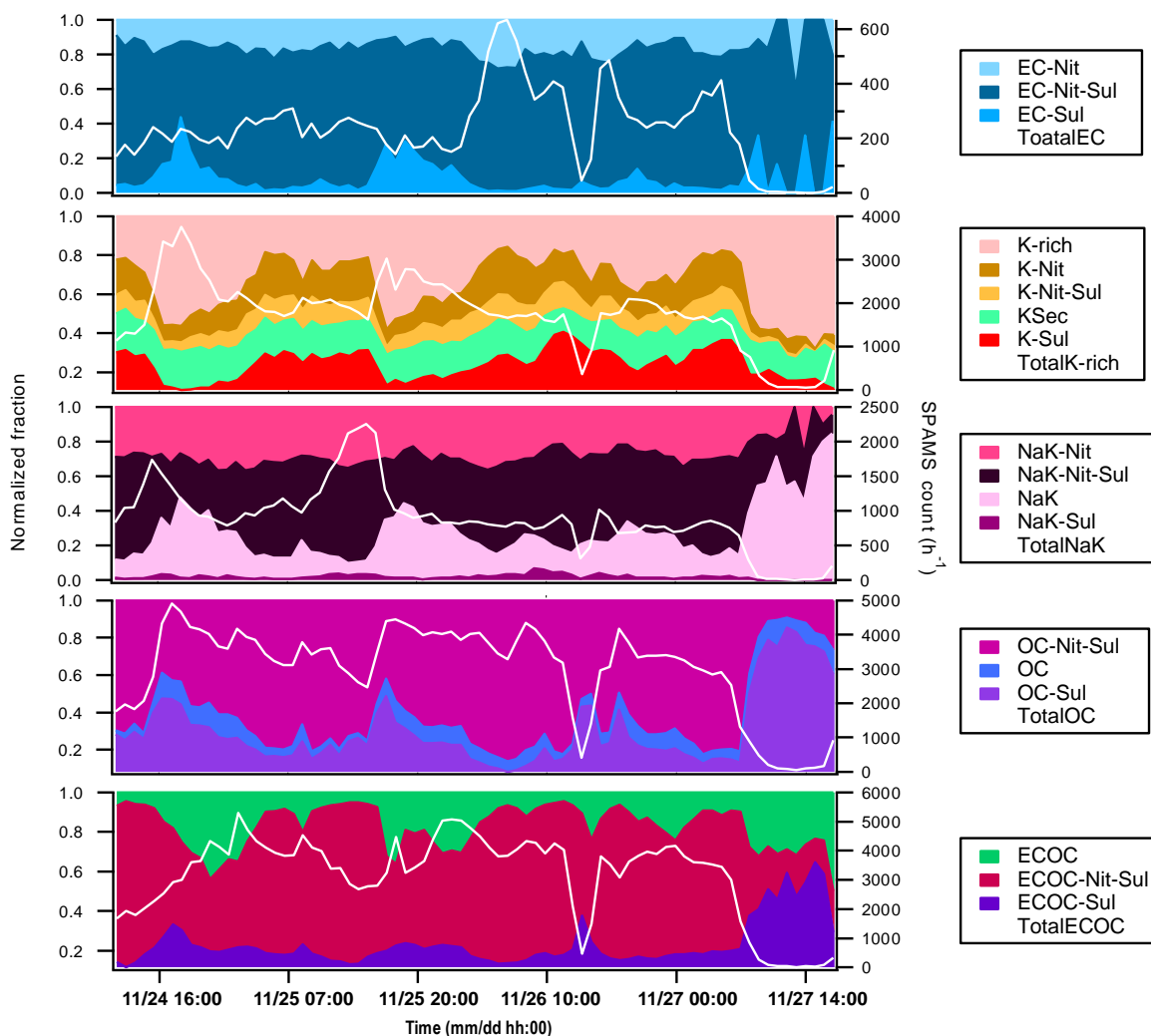
286 Sul, which came from the west, i.e., urban Beijing, was pronounced, while at PKU, aged  
287 particle types such as OC-Nit-Sul, K-Nit-Sul, K-Nit, NaK-Nit, and K-Nit-Sul increased  
288 dramatically due to transport. These particle types were emitted from residential heating in  
289 rural areas. In the accumulation stages at both sites, the concentrations of local particles  
290 rose, such as EC-Nit-Sul at PKU and NaK-Nit-Sul at PG. In short, the evolution of particles,  
291 including both transport and accumulation at both PKU and PG, were affected by the  
292 movement of air mass and local emissions.

293 When E4\_PG occurred, transport from the southwest was identified along with the  
294 transport of EC-Sul and EC-Nit-Sul, resulting in a PM<sub>2.5</sub> concentration of 176  $\mu\text{g m}^{-3}$  at  
295 10:00 on 11/24/2016. The average wind speed was 1.5  $\text{ms}^{-1}$  at the time, representing a  
296 typical stagnant-air condition. All particle families showed accumulation trends after that  
297 (Figure 4). The sharp decrease of all particle families was due to the high western wind  
298 speed ( $> 4 \text{ ms}^{-1}$ ) at 12:00 on 11/26/2016. During particulate accumulation at PG, such local  
299 particle types as ECOC, OC, and NaK still had diurnal patterns, but the aged “-Nit-Sul”  
300 particles types were predominant ( $> 50\%$  in all particle families). Thus, the local  
301 accumulation of pollutants was the major driver of E4\_PG (Figure 8).



302

303 Figure 8. Time trends of number fractions of particle types (left) and  
 304 particle families (EC, BB, NaK, OC, and ECOC, right) during Pollution Event 1 (E1 11/01–  
 305 11/08) at PG.



306

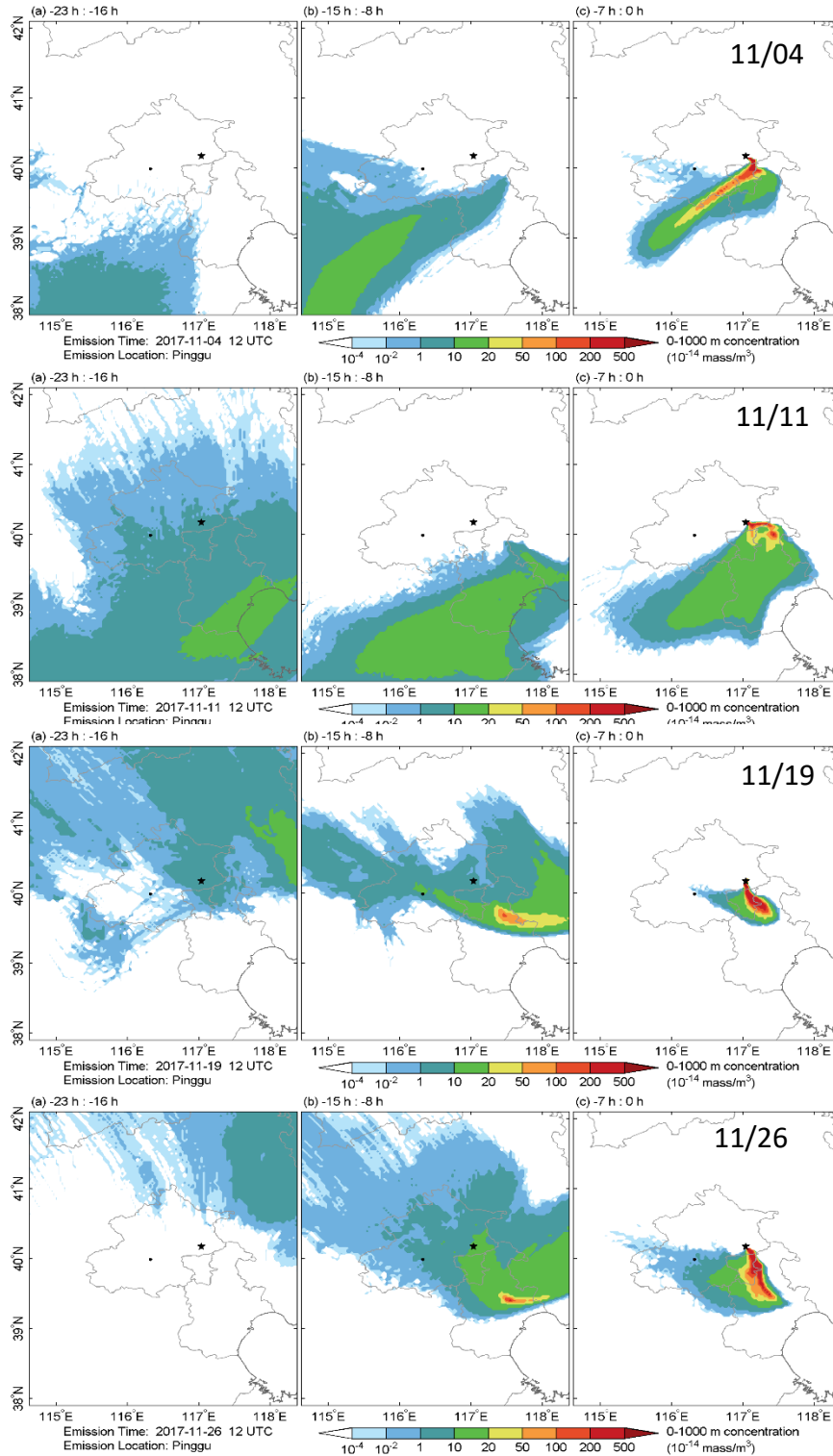
307 Figure 9. Time trends of number fractions of particle types (left) and hourly counts of  
 308 particle families (EC, BB, NaK, OC, and ECOC, right) during Pollution Event 4 (E4) at  
 309 PG.

### 310 3.6 Interaction of PM between PKU and PG

311 Since PKU and PG share 17 common particle types, possible transport between the two  
 312 sites was validated using the HYSPLIT model. All cases of transport are available in  
 313 Supplementary information (Figures S11 and S12). Figures 10 and 11 only illustrate the  
 314 examples of transport during each pollution event. The PKU site is located on the edge of

315 plumes originating from PG during E1, which implies that the particulate transport was  
316 partially from PG (Figure 10). Moreover, the PKU site lies in the high concentration zone  
317 of plumes PG from during E3 and E4. Therefore, E3\_PKU and E4\_PKU were confidently  
318 considered input haze events. In contrast, the relatively slighter transport of air mass from  
319 PKU to PG was observed during these events. As shown in Figure 11, the air mass passing  
320 through the PKU site mainly influenced the areas in the south and east. Consequently, the  
321 PG site was seldom in the high concentration zone of plumes originating from PKU.

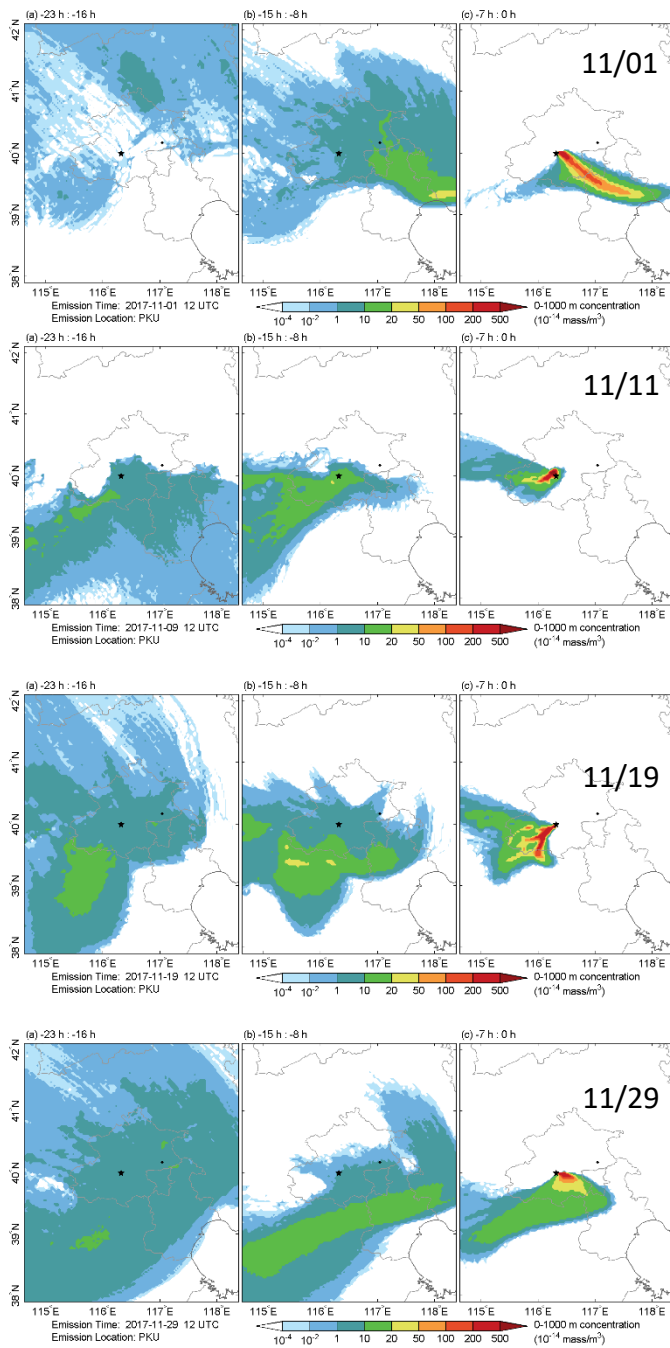
322 Figures 10 and 11 suggest that pollutants were transported significantly from PG to PKU  
323 during stagnant air conditions when dense haze occurred. These results are consistent with  
324 the analysis of particle categories. *As shown in Figure 3, when the transport occurred in*  
325 *04<sup>th</sup> November, 19<sup>th</sup> November, and 26 November, the regional particle types, such as K-*  
326 *Nit-Sul, Nak-Nit-Sul, ECOC-Nit-Sul, and OC-Nit-Sul increased due to the transport from*  
327 *the East (Part I).* In an urban area such as PKU, the local EC particles were associated with  
328 the ECOC and OC families causing severe pollution in the urban area. On the other hand,  
329 in the rural area, the aged particles were dominant under stagnant air conditions and  
330 transported to PKU, leading to extreme urban particulate pollution. Besides, our results are  
331 consistent with other studies in the APHH-Beijing Project. For example, Du et al. (2019)  
332 have confirmed that regional transport plays a non-negligible role in haze episodes with  
333 contributions of 14–31% to the surface PM<sub>2.5</sub> mass concentration.



334

335 Figure 10. Typical dispersion of air mass from PG (star, on the right) to PKU (dot, on the  
 336 left) during E1 (11/04), E2 (11/11), E3 (11/19) and E4 (11/26).





337

338 Figure 11. Typical dispersion of air mass from PKU (star, on the left) to PG (dot, on the  
 339 right) in E1 (11/01), E2 (11/11), E3 (11/19) and E4 (11/29).

### 340 **3.7 Implications**

341 This study provides the polar plots that are used to explain the interaction of pollutants and  
342 wind. Such regional pollution sources as BB, coal, and steel industries have a strong impact  
343 on the particulate chemical composition of the air in urban Beijing. Besides, according to  
344 model studies, [air pollutants in Hebei, Henan, and Shandong provinces](#) are transported to  
345 Beijing (Shi et al., 2019; Du et al., 2019). In these provinces, efforts have been made to  
346 abate emissions from the steel industry, power plants, and traffic. However, BB accounted  
347 for 10–20% of the PM<sub>2.5</sub> in the study period (Liu et al., 2019). In particular, household  
348 biofuel combustion is a primary BB source during winter, impacting both outdoor and  
349 indoor air quality (Zhang and Cao, 2015). Therefore, more attention should be paid to  
350 tackling BB emissions.

351 This study improves our general understanding of the sources of sulfates in Beijing.  
352 Particles that only increased with the uptake of sulfate, such as OC-Sul\_PKU, K-Sul\_PKU,  
353 and NaK-Sul\_PKU, were transported regionally and arrived at the sampling site during  
354 high wind speeds ( $> 4 \text{ m s}^{-1}$ ). The results are consistent with the findings of Duan et al.  
355 (2019) and Du et al. (2019) that sulfates in Beijing during winter are formed regionally.  
356 Nitrate-containing particles could be found after processing in the NO<sub>x</sub>-rich urban and rural  
357 plumes of Beijing. Since SPAMS is limited in tracking such partial organics as  
358 hydrocarbons and PAHs, the evolution of secondary organics is unavailable in this study.

### 359 **4. Summary**

360 The wintertime haze events that occurred in Beijing from 11/01/2016 to 11/29/2016 have  
361 been investigated. The heating period, including central and residential heating in both

362 urban and rural areas, severely impacted the particulate chemical composition in the region.  
363 In Beijing, a pattern of the transport and accumulation of particles was found in both the  
364 urban and rural areas. *The input of regional particles was strongly connected to stagnation  
365 of the air which provided favorable conditions for the accumulation of pollutants,  
366 ultimately leading to severe haze events.* In the rural area, the heavy haze was mainly  
367 controlled by air stagnation and local emissions, but regional transport was also observed.  
368 We also discussed the influence of regional transport using the dispersion model. The air  
369 masses between PKU and PG interacted with each other whenever heavy haze occurred.  
370 Parts I and II of this study are useful for understanding the formation mechanism of winter  
371 haze in both the urban and rural areas of Beijing. This study also implies that the mitigation  
372 of PM relies on both urban and rural areas.

373 *Data availability.* All the data described in this study is available upon request from the  
374 corresponding authors.

375 *Author contributions.* YC, FY, MZ, TZ, and KH designed the experiments; YC, JC, ZW,  
376 MT, CP, and HY carried them out; XY, GS, and SZ analyzed the experimental data; YC  
377 prepared the manuscript with contributions from all coauthors.

378 *Competing interests.* The authors declare that they have no conflicts of interest.

379 *Acknowledgments.* We are grateful for financial support from the National Natural Science  
380 Foundation of China (Grant No. 41703136 and 81571130100).

381

382 References

383 Chagger, H., Jones, J., Pourkashanian, M., Williams, A., Owen, A., and Fynes, G.:  
384 Emission of volatile organic compounds from coal combustion, *Fuel*, 78, 1527-1538, 1999.

385 Che, H., Xia, X., Zhu, J., Li, Z., Dubovik, O., Holben, B., Goloub, P., Chen, H., Estelles,  
386 V., Cuevas-Agulló, E., Blarel, L., Wang, H., Zhao, H., Zhang, X., Wang, Y., Sun, J., Tao,  
387 R., Zhang, X., and Shi, G.: Column aerosol optical properties and aerosol radiative forcing  
388 during a serious haze-fog month over North China Plain in 2013 based on ground-based  
389 sunphotometer measurements, *Atmos. Chem. Phys.*, 14, 2125-2138, 10.5194/acp-14-2125-  
390 2014, 2014.

391 Chen, Y., Ebenstein, A., Greenstone, M., and Li, H.: Evidence on the impact of sustained  
392 exposure to air pollution on life expectancy from China's Huai River policy, *Proceedings*  
393 *of the National Academy of Sciences*, 110, 12936-12941, 2013.

394 Chen, Y., Cao, J., Huang, R., Yang, F., Wang, Q., and Wang, Y.: Characterization, mixing  
395 state, and evolution of urban single particles in Xi'an (China) during wintertime haze days,  
396 *Sci. Total Environ.*, 573, 937-945, 10.1016/j.scitotenv.2016.08.151, 2016a.

397 Chen, Y., Schleicher, N., Fricker, M., Cen, K., Liu, X. L., Kaminski, U., Yu, Y., Wu, X.  
398 F., and Norra, S.: Long-term variation of black carbon and PM<sub>2.5</sub> in Beijing, China with  
399 respect to meteorological conditions and governmental measures, *Environ. Pollut.*, 212,  
400 269-278, 10.1016/j.envpol.2016.01.008, 2016b.

401 Chen, Y., Liu, H., Yang, F., Zhang, S., Li, W., Shi, G., Wang, H., Tian, M., Liu, S., Huang,  
402 R., Wang, Q., Wang, P., and Cao, J.: Single particle characterization of summertime

403 particles in Xi'an (China), *Sci. Total Environ.*, 636, 1279-1290,  
404 10.1016/j.scitotenv.2018.04.388, 2018.

405 Chen, Y., Liu, H., Huang, R. J., Yang, F., Tian, M., Yao, X., Shen, Z., Yan, L., and Cao,  
406 J.: Atmospheric Processing of Loess Particles in a Polluted Urban Area of Northwestern  
407 China, *J. Geophys. Res. Atmos.*, 124, 7919-7929, 10.1029/2018jd029956, 2019a.

408 Chen, Y., Tian, M., Huang, R.-J., Shi, G., Wang, H., Peng, C., Cao, J., Wang, Q., Zhang,  
409 S., Guo, D., Zhang, L., and Yang, F.: Characterization of urban amine-containing particles  
410 in southwestern China: seasonal variation, source, and processing, *Atmos. Chem. Phys.*,  
411 19, 3245-3255, 10.5194/acp-19-3245-2019, 2019b.

412 Chen, Y., Cai, J., Wang, Z., Peng, C., Yao, X., Tian, M., Han, Y., Shi, G., Shi, Z., Liu, Y.,  
413 Yang, X., Zheng, M., Zhu, T., He, K., Zhang, Q., and Yang, F.: Simultaneous Measurement  
414 of Urban and Rural Single Particles in Beijing, Part I: Chemical Composition and Mixing  
415 State, *Atmos. Chem. Phys. Discuss.*, 2020, 1-40, 10.5194/acp-2019-933, 2020.

416 Cheng, Y., Zheng, G., Wei, C., Mu, Q., Zheng, B., Wang, Z., Gao, M., Zhang, Q., He, K.,  
417 and Carmichael, G.: Reactive nitrogen chemistry in aerosol water as a source of sulfate  
418 during haze events in China, *Science Advances*, 2, e1601530, 2016.

419 Du, H., Li, J., Chen, X., Wang, Z., Sun, Y., Fu, P., Li, J., Gao, J., and Wei, Y.: Modeling  
420 of aerosol property evolution during winter haze episodes over a megacity cluster in  
421 northern China: roles of regional transport and heterogeneous reactions of SO<sub>2</sub>, *Atmos.*  
422 *Chem. Phys.*, 19, 9351-9370, 10.5194/acp-19-9351-2019, 2019.

423 Duan, J., Huang, R. J., Lin, C., Dai, W., Wang, M., Gu, Y., Wang, Y., Zhong, H., Zheng,  
424 Y., Ni, H., Dusek, U., Chen, Y., Li, Y., Chen, Q., Worsnop, D. R., O'Dowd, C. D., and

425 Cao, J.: Distinctions in source regions and formation mechanisms of secondary aerosol in  
426 Beijing from summer to winter, *Atmos. Chem. Phys.*, 19, 10319-10334, 10.5194/acp-19-  
427 10319-2019, 2019.

428 Guo, S., Hu, M., Zamora, M. L., Peng, J., Shang, D., Zheng, J., Du, Z., Wu, Z., Shao, M.,  
429 Zeng, L., Molina, M. J., and Zhang, R.: Elucidating severe urban haze formation in China,  
430 *Proc. Natl. Acad. Sci. U.S.A.*, 111, 17373-17378, 10.1073/pnas.1419604111, 2014.

431 He, H., Tie, X., Zhang, Q., Liu, X., Gao, Q., Li, X., and Gao, Y.: Analysis of the causes of  
432 heavy aerosol pollution in Beijing, China: A case study with the WRF-Chem model,  
433 *Particuology*, 20, 32-40, 2015.

434 Lee, R. G., Coleman, P., Jones, J. L., Jones, K. C., and Lohmann, R.: Emission factors and  
435 importance of PCDD/Fs, PCBs, PCNs, PAHs and PM10 from the domestic burning of coal  
436 and wood in the UK, *Environ. Sci. Technol.*, 39, 1436-1447, 2005.

437 Li, L., Huang, Z., Dong, J., Li, M., Gao, W., Nian, H., Fu, Z., Zhang, G., Bi, X., Cheng, P.,  
438 and Zhou, Z.: Real time bipolar time-of-flight mass spectrometer for analyzing single  
439 aerosol particles, *Int. J. Mass spectrom.*, 303, 118-124, 10.1016/j.ijms.2011.01.017, 2011.

440 Li, P., Yan, R., Yu, S., Wang, S., Liu, W., and Bao, H.: Reinstate regional transport of  
441 PM2.5 as a major cause of severe haze in Beijing, *Proc. Natl. Acad. Sci. U.S.A.*, 112, 2015.

442 Li, W., Shao, L., Zhang, D., Ro, C.-U., Hu, M., Bi, X., Geng, H., Matsuki, A., Niu, H., and  
443 Chen, J.: A review of single aerosol particle studies in the atmosphere of East Asia:  
444 morphology, mixing state, source, and heterogeneous reactions, *J Clean Prod*, 112, 1330-  
445 1349, 10.1016/j.jclepro.2015.04.050, 2016.

446 Linak, W. P., Yoo, J.-I., Wasson, S. J., Zhu, W., Wendt, J. O. L., Huggins, F. E., Chen, Y.,  
447 Shah, N., Huffman, G. P., and Gilmour, M. I.: Ultrafine ash aerosols from coal combustion:  
448 Characterization and health effects, *Proceedings of the Combustion Institute*, 31, 1929-  
449 1937, 10.1016/j.proci.2006.08.086, 2007.

450 Liu, Y., Zheng, M., Yu, M., Cai, X., Du, H., Li, J., Zhou, T., Yan, C., Wang, X., Shi, Z.,  
451 Harrison, R. M., Zhang, Q., and He, K.: High-time-resolution source apportionment of  
452 PM<sub>2.5</sub> in Beijing with multiple models, *Atmos. Chem. Phys.*, 19, 6595-6609, 10.5194/acp-  
453 19-6595-2019, 2019.

454 Ma, L., Li, M., Huang, Z., Li, L., Gao, W., Nian, H., Zou, L., Fu, Z., Gao, J., Chai, F., and  
455 Zhou, Z.: Real time analysis of lead-containing atmospheric particles in Beijing during  
456 springtime by single particle aerosol mass spectrometry, *Chemosphere*, 154, 454-462,  
457 10.1016/j.chemosphere.2016.04.001, 2016.

458 Quan, J., Gao, Y., Zhang, Q., Tie, X., Cao, J., Han, S., Meng, J., Chen, P., and Zhao, D.:  
459 Evolution of planetary boundary layer under different weather conditions, and its impact  
460 on aerosol concentrations, *Particuology*, 11, 34-40, 10.1016/j.partic.2012.04.005, 2013.

461 Shi, Z., Vu, T., Kotthaus, S., Harrison, R. M., Grimmond, S., Yue, S., Zhu, T., Lee, J., Han,  
462 Y., Demuzere, M., Dunmore, R. E., Ren, L., Liu, D., Wang, Y., Wild, O., Allan, J., Acton,  
463 W. J., Barlow, J., Barratt, B., Beddows, D., Bloss, W. J., Calzolari, G., Carruthers, D.,  
464 Carslaw, D. C., Chan, Q., Chatzidiakou, L., Chen, Y., Crilley, L., Coe, H., Dai, T., Doherty,  
465 R., Duan, F., Fu, P., Ge, B., Ge, M., Guan, D., Hamilton, J. F., He, K., Heal, M., Heard,  
466 D., Hewitt, C. N., Hollaway, M., Hu, M., Ji, D., Jiang, X., Jones, R., Kalberer, M., Kelly,  
467 F. J., Kramer, L., Langford, B., Lin, C., Lewis, A. C., Li, J., Li, W., Liu, H., Liu, J., Loh,  
468 M., Lu, K., Lucarelli, F., Mann, G., McFiggans, G., Miller, M. R., Mills, G., Monk, P.,

469 Nemitz, E., O'Connor, F., Ouyang, B., Palmer, P. I., Percival, C., Popoola, O., Reeves, C.,  
470 Rickard, A. R., Shao, L., Shi, G., Spracklen, D., Stevenson, D., Sun, Y., Sun, Z., Tao, S.,  
471 Tong, S., Wang, Q., Wang, W., Wang, X., Wang, X., Wang, Z., Wei, L., Whalley, L., Wu,  
472 X., Wu, Z., Xie, P., Yang, F., Zhang, Q., Zhang, Y., Zhang, Y., and Zheng, M.: Introduction  
473 to the special issue “In-depth study of air pollution sources and processes within Beijing  
474 and its surrounding region (APHH-Beijing)”, *Atmos. Chem. Phys.*, 19, 7519-7546,  
475 10.5194/acp-19-7519-2019, 2019.

476 Sun, Y., Wang, Z., Fu, P., Jiang, Q., Yang, T., Li, J., and Ge, X.: The impact of relative  
477 humidity on aerosol composition and evolution processes during wintertime in Beijing,  
478 China, *Atmos. Environ.*, 77, 927-934, 10.1016/j.atmosenv.2013.06.019, 2013a.

479 Sun, Y., Wang, Z., Fu, P., Yang, T., Jiang, Q., Dong, H., Li, J., and Jia, J.: Aerosol  
480 composition, sources and processes during wintertime in Beijing, China, *Atmos. Chem.*  
481 *Phys.*, 13, 4577-4592, 2013b.

482 Sun, Y., Jiang, Q., Wang, Z., Fu, P., Li, J., Yang, T., and Yin, Y.: Investigation of the  
483 sources and evolution processes of severe haze pollution in Beijing in January 2013, *J.*  
484 *Geophys. Res. Atmos.*, 119, 4380-4398, 10.1002/2014jd021641, 2014.

485 Tian, S., Pan, Y., Liu, Z., Wen, T., and Wang, Y.: Size-resolved aerosol chemical analysis  
486 of extreme haze pollution events during early 2013 in urban Beijing, China, *J Hazard Mater*,  
487 279, 452-460, 2014.

488 Wang, G., Zhang, R., Gomez, M. E., Yang, L., Levy Zamora, M., Hu, M., Lin, Y., Peng,  
489 J., Guo, S., Meng, J., Li, J., Cheng, C., Hu, T., Ren, Y., Wang, Y., Gao, J., Cao, J., An, Z.,  
490 Zhou, W., Li, G., Wang, J., Tian, P., Marrero-Ortiz, W., Secretst, J., Du, Z., Zheng, J.,



491 Shang, D., Zeng, L., Shao, M., Wang, W., Huang, Y., Wang, Y., Zhu, Y., Li, Y., Hu, J.,  
492 Pan, B., Cai, L., Cheng, Y., Ji, Y., Zhang, F., Rosenfeld, D., Liss, P. S., Duce, R. A., Kolb,  
493 C. E., and Molina, M. J.: Persistent sulfate formation from London Fog to Chinese haze,  
494 Proc. Natl. Acad. Sci. U.S.A., 113, 13630-13635, 10.1073/pnas.1616540113, 2016.

495 Wang, J., Liu, D., Ge, X., Wu, Y., Shen, F., Chen, M., Zhao, J., Xie, C., Wang, Q., Xu, W.,  
496 Zhang, J., Hu, J., Allan, J., Joshi, R., Fu, P., Coe, H., and Sun, Y.: Characterization of black  
497 carbon-containing fine particles in Beijing during wintertime, Atmos. Chem. Phys., 19,  
498 447-458, 10.5194/acp-19-447-2019, 2019.

499 Wu, J., Bei, N., Hu, B., Liu, S., Zhou, M., Wang, Q., Li, X., Liu, L., Feng, T., Liu, Z.,  
500 Wang, Y., Cao, J., Tie, X., Wang, J., Molina, L. T., and Li, G.: Aerosol–radiation feedback  
501 deteriorates the wintertime haze in the North China Plain, Atmos. Chem. Phys., 19, 8703-  
502 8719, 10.5194/acp-19-8703-2019, 2019.

503 Xu, J., Wang, H., Li, X., Li, Y., Wen, J., Zhang, J., Shi, X., Li, M., Wang, W., Shi, G., and  
504 Feng, Y.: Refined source apportionment of coal combustion sources by using single  
505 particle mass spectrometry, Sci. Total Environ., 627, 633-646,  
506 10.1016/j.scitotenv.2018.01.269, 2018.

507 Zhang, J., Huang, X., Chen, Y., Luo, B., Luo, J., Zhang, W., Rao, Z., and Yang, F.:  
508 Characterization of lead-containing atmospheric particles in a typical basin city of China:  
509 Seasonal variations, potential source areas, and responses to fireworks, Sci. Total Environ.,  
510 661, 354-363, 10.1016/j.scitotenv.2019.01.079, 2019.

511 Zhang, L., Wang, T., Lv, M., and Zhang, Q.: On the severe haze in Beijing during January  
512 2013: Unraveling the effects of meteorological anomalies with WRF-Chem, *Atmos.*  
513 *Environ.*, 104, 11-21, 10.1016/j.atmosenv.2015.01.001, 2015.

514 Zhang, Y., Chen, J., Yang, H., Li, R., and Yu, Q.: Seasonal variation and potential source  
515 regions of PM<sub>2.5</sub>-bound PAHs in the megacity Beijing, China: Impact of regional transport,  
516 *Environ. Pollut.*, 231, 329-338, 10.1016/j.envpol.2017.08.025, 2017.

517 Zhang, Y. L., and Cao, F.: Is it time to tackle PM(2.5) air pollutions in China from biomass-  
518 burning emissions?, *Environ. Pollut.*, 202, 217-219, 10.1016/j.envpol.2015.02.005, 2015.

519 Zhong, J., Zhang, X., Wang, Y., Sun, J., Zhang, Y., Wang, J., Tan, K., Shen, X., Che, H.,  
520 Zhang, L., Zhang, Z., Qi, X., Zhao, H., Ren, S., and Li, Y.: Relative contributions of  
521 boundary-layer meteorological factors to the explosive growth of PM<sub>2.5</sub> during the red-  
522 alert heavy pollution episodes in Beijing in December 2016, *Journal of Meteorological*  
523 *Research*, 31, 809-819, 10.1007/s13351-017-7088-0, 2017.

524